

Supporting Information
©Wiley-VCH 2021
69451 Weinheim, Germany

**“Turbo-Charged” DNA Motors with Optimized Sequence Enable
Single-Molecule Nucleic Acid Sensing**

Luona Zhang⁺, Selma Piranej⁺, Arshiya Namazi, Steven Narum, Khalid Salaita^{*}

Table of Contents

S1: Materials and Methods

S2: Supplementary Notes

S3: Supplementary Data: Supplementary Table 1, Supplementary Figures 1-19

S4: Supplementary Movies

References

S1. Materials and methods

1. Materials

1.1 Reagents

All chemicals were purchased from Sigma-Aldrich unless otherwise stated. All oligonucleotides were custom synthesized by Integrated DNA Technologies, stored at 4 °C (−30 °C for RNA) and used without purification. Their sequences, including functional group modifications, are listed in Supplementary Table 1. Stock solutions were prepared using Nanopure water (Barnstead Nanopure System, resistivity = 18.2 MΩ), herein referred to as DI water. Aminated silica beads (5 μm diameter) were purchased from Bangs Laboratory (SA06N). RNase H was obtained from Takara Clontech (2150A). Thin gold films were generated using a home-built thermal evaporator system. All particle translocation measurements were performed in ibidi sticky-Slide VI^{0.4} 17 × 3.8 × 0.4 mm³ channels.

2. Methods

2.1 Optical microscopy

Bright-field and fluorescence images were acquired on a fully automated Eclipse Ti2-E Nikon Inverted Research Microscope using the Elements software package (Nikon). The microscope was equipped with an automated scanning stage, a 1.49 NA CFI Apo TIRF ×100 objective, a 0.50 NA CFI60 Plan Fluor ×20 objective, a Prime 95B 25 mm scientific complementary metal oxide semiconductor (sCMOS) camera for image capture at 16-bit depth, a SOLA SE II 365 Light Engine as a solid-state white-light excitation source and a *Perfect Focus System* used to prevent loss of focus during time-lapses. Fluorescence images of cyanine dye Cy3 were collected using a TRITC filter set (Chroma, 96321) with an exposure time of 100 ms. Fluorescence images of ATTO647N labelled SNAs were collected using CY5/AlexaFluor 647/DraQ5 filter set with an exposure time of 1s. All imaging was conducted at room temperature.

2.2 Thermal evaporation of gold films

A No. 1.5H glass coverslip with dimensions 25 × 75 mm² (ibidi, 10812) was cleaned by sonication in 200 proof ethanol (Fisher Scientific, 04-355-223) for at least 15 min. The sample was then dried in an oven for at least 30 min. The cleaned glass coverslip was then mounted in a home-built thermal evaporator chamber in which the pressure was reduced to 50 × 10^{−3} torr. The chamber was purged with N₂ three times, and the pressure was reduced to (1-2) × 10^{−7} torr using a turbo pump with a liquid N₂ trap. Once the desired pressure had been achieved, a 3-nm film of Cr was deposited onto the slide at a rate of 0.2 Å s^{−1}, which was determined by a quartz crystal microbalance. After the Cr adhesive layer had been deposited, 5-nm layer of Au was deposited at a rate of 0.3 Å s^{−1}. The Au-coated samples were used within 1 week of deposition.

2.3 Fabrication of RNA monolayers

A sticky-Slide VI^{0.4} flow chamber (ibidi, 80608) was adhered to the Au-coated slide to produce six channels (17 × 3.8 × 0.4 mm³). Prior to surface functionalization, the channels were rinsed with ~10 ml DI water. Next, thiol-modified DNA anchor strands were added to each of the channels using a 50 μl solution of 1 μM DNA anchor in 1 M KHPO₄ buffer. The gold film was sealed with Parafilm to prevent evaporation, with the reaction taking place overnight at room temperature. After incubation, excess DNA was removed from the channels by rinsing with ~10 ml DI water. To block any bare gold sites and to maximize the hybridization of RNA to the DNA anchoring strands, the surface was backfilled with 100 μl of a 100 μM solution of 11-(mercaptoundecyl) hexa(ethylene glycol) (SH-PEG; Sigma-Aldrich, 675105) solution in ethanol for 6 h. Excess SH-PEG was removed by rinsing with ~10 ml DI water. Then, 100 μl of 100 nM RNA/DNA chimera was added to the surface through hybridization in 1x PBS overnight for 12 h. For the surface-bound DNA probes sensing experiments, DNA strands analog to the RNA were mixed with the RNA/DNA chimera at different ratios while keeping the combined concentration of 100 nM constant. The channels were again sealed with Parafilm to prevent evaporation and the resulting RNA monolayer remained stable for days, as determined by fluorescence imaging.

The TOI sensing experiments consisted of similar surface preparation procedures except for the RNA/DNA chimera step. Following the incubation with 100 μl of 100 μM SH-PEG, the surface was incubated with a binary mixture of RNA/DNA chimera and target DNA. For example, the 500 probes/μm² surface was functionalized with 99 nM of RNA/DNA chimera and 1 nM of target DNA in 1x PBS and subsequent dilutions followed for the rest of the surfaces (50, 5, and 0.5 probes/μm²).

2.4 Determination of RNase H surface kinetics

A monolayer of RNA/DNA duplexes was generated by hybridizing a soluble complementary DNA strand to the RNA monolayer. Briefly, 100 μ l of a DNA stock solution (100 nM) in 1x PBS was added to the ssRNA surface. After 24 hours of hybridization, the excess DNA was washed away by rinsing the channel with 1 ml 1x PBS, which was exchanged for 100 μ l of RNase H reaction buffer (10 μ M DTT, 25 mM Tris pH 8, 37.5 mM KCl, 1.5 mM MgCl₂ and 0.75% w/v Triton X) containing 5 units of RNase H and different concentrations of formamide. The reaction progress was monitored by measuring the loss in surface Cy3 fluorescence over time. After background subtraction and normalization to the initial intensity, the data was fitted to an exponential decay function to report the half-life.

2.5 Synthesis of azide-functionalized particles

First, the aminated silica were washed to remove any impurities. 1 mg of aminated silica beads were suspended in 1 ml DI water and centrifuged for 5 min at 15,000 r.p.m. in. The supernatant was discarded, and the resulting particles were resuspended in 1 ml DI water. This was repeated three times, and the supernatant was discarded after the final wash. The azide-functionalized particles were then synthesized by mixing the aminated silica with 1 mg azidoacetic N-hydroxysuccinimide ester (BroadPharm, BP-22467). This mixture was subsequently diluted in 100 μ l dimethylsulfoxide (DMSO) and 1 μ l of a tenfold-diluted triethylamine stock solution in DMSO. The reaction was allowed to proceed overnight for 24 h at room temperature. The resulting azide-modified silica particles were then purified by adding 1 ml DI water and centrifuging the particles at 15,000 r.p.m. for 5 min. The supernatant was discarded, and the resulting particles were resuspended in 1 ml DI water. This process was repeated seven times, and after the final centrifugation step the particles were resuspended in 50 μ l DI water. The azide-modified particle stock was stored at 4 °C in the dark and used within one month of preparation.

2.6 Synthesis of DNA-functionalized particles

High-density DNA-functionalized particles were synthesized by adding 5 nanomoles (in 5 μ l) of alkyne-modified DNA stock solution to 5 μ l of azide-functionalized particles. This mixture was diluted with 25 μ l of DMSO and 5 μ l of a 2 M triethyl ammonium acetate buffer (pH 7.0). Next, 4 μ l of a supersaturated stock solution of ascorbic acid was added to the reaction as a reducing agent. Cycloaddition between the alkyne-modified DNA and azide-functionalized particles was initiated by adding 2 μ l of a 10 mM copper tris[(1-benzyl-1H-1,2,3-triazol-4-yl)methyl]amine (Cu-TBTA) stock solution in 55 vol% DMSO (Lumiprobe, 21050). The reaction was incubated for 24 hours at room temperature and the resulting DNA-functionalized particles were purified by centrifugation. Specifically, the particles were centrifuged at 15,000 r.p.m. for five minutes, after which the supernatant was discarded, and the particles resuspended in 1 ml of a 1x PBS and 10% (w/v) Triton-X solution. This process was repeated seven times, with the particles resuspended in 1 ml 1x PBS only for the fourth to sixth centrifugations. After the final centrifugation, the particles were resuspended in 50 μ l of 1x PBS buffer. The high-density DNA-functionalized particles were stored at 4 °C and protected from light.

2.7 Particle translocation

Initially, the RNA monolayer was washed with 1 ml of 1x PBS to remove excess unbound RNA. The quality of the RNA monolayer in each well was checked for homogeneity and intensity (~10,000 a.u. is typical). Next, DNA-functionalized particles were hybridized to the RNA-substrate surface. Briefly, 5 μ l of DNA-functionalized particles were diluted with 45 μ l of 1x PBS and introduced into the reaction chamber. Hybridization between the particles and the complementary RNA monolayer occurred over an incubation period of 10 min. Particle translocation was initiated by buffer exchange with 100 μ l of rolling buffer consisting of water, 0.75% (w/v) Triton-X in water, 0.5x RNase H buffer (25 mM Tris pH 8, 37.5 mM KCl, 1.5 mM MgCl₂) and 10 μ M DTT. A range between 1 to 10 units of RNase H was added last to the rolling buffer: 1 μ l of the RNase H stock solution (60 units/ μ l) was diluted with 11 μ l of 1x PBS and stored on ice for up to 2 h (1 μ l of this dilution contains 5 U RNase H). A final concentration of 30%, 10% and 0% formamide (%v/v) was used in the 100%, 33%, and 0% GC designs, respectively. Particle translocation was monitored through bright-field imaging ($\times 20$) by time-lapse acquisition at intervals of 5 s for 30 min using the Nikon Elements software. High-resolution epifluorescence images ($\times 100$) of fluorescence-depletion tracks were acquired to verify that particle motion resulted from processive RNA hydrolysis. For high-resolution movies ($\times 100$), both bright-field and epifluorescence images were recorded at five second intervals.

2.8 Labeling DNA strands with dyes

Aminated DNA strand (100 μ M) was mixed with excess ATTO647-NHS ester (500 μ g/ml) in DMSO, 10 μ l of 10x PBS and 10 μ l of 1 M NaHCO₃. The mixture was allowed to react for 1.5 hours at room temperature. The product was then filtered by P2 gel to remove salts and unreacted dyes and purified by HPLC. (solvent A: 0.1 M TEAA, solvent B: 100% MeCN; initial condition was 10% B with a gradient of 1% per min, flow rate: 0.5 ml/min).

2.9 DNA functionalization of gold nanoparticles

Gold nanoparticles were functionalized with DNA following the freeze method.^[1] Thiolated DNA with ATTO647N were added in 350-fold excess to 15-nm gold nanoparticles, and frozen at -30 °C for at least one hour. Immediately after removing the gold nanoparticles from the freezer, 10x PBS was added to create a final concentration of 1x PBS and was thawed for 30 minutes. Following the thaw, the solution was brought up to 500 μ L using 1x PBS before being centrifuged at 13,000 g for 20 minutes at room temperature (Eppendorf Centrifuge 5424 R). Unbound DNA was removed via aspiration, and the gold nanoparticle solution was washed and centrifuged a total of three times. DNA functionalized gold nanoparticles (spherical nucleic acids or SNA) were stored at 4 °C for up to one week until use. Before experimentation, the concentration was determined through UV-Vis spectroscopy by measuring the peak absorbance (~527 nm) and using Beer-Lambert's Law.

2.10 Using SNAs for probe visualization

After the SNAs were synthesized, each of the RNA surfaces functionalized with different TOI probe density was incubated overnight with 10 nM SNAs in 1x PBS. Following incubation, the unbound SNAs were washed with 1 ml of 1x PBS and imaged using the ATTO647N fluorescence channel.

2.11 Image processing and particle tracking

Image processing and particle tracking were performed in Fiji (ImageJ) as well as in Python. The bioformats toolbox enabled direct transfer of Nikon Elements image files (*.nd2) into the Fiji (ImageJ) environment where all image/video processing was performed. BIG-EPFL StackReg and MOSAIC ImageJ plugins were used for drift correction and particle tracking, respectively. The algorithms processing the data for motor trajectories, net displacements and velocities were performed using a custom Python code adapted for Google colab (https://colab.research.google.com/). Calculation of additional drift correction was adapted from trackpy (https://soft-matter.github.io/trackpy/v0.4.2/). Full Python script from bright-field acquisition data can be found at https://github.com/luona-zhang/Rolling-DNA-motors-motion-analysis. Statistical analyses were performed in GraphPad (v. 9.5.1) using one-way ANOVA ("analysis of variance").

S2. Supplementary Notes

The encounter rate and time to probe encounter were calculated using the following inputs:

- Rolling experiment condition:
0% GC motors at 0.01 U/ μ l RNase H and 0% v/v formamide
- Average speed (tripl.)=39.10 nm/s

$$k_{\text{encounter}} = 50,000 \frac{\text{strands}}{\mu\text{m}^2} \times 0.0391 \frac{\mu\text{m}}{\text{s}} \times 0.2 \times 0.4 \mu\text{m} \approx 156 \frac{\text{strands}}{\text{s}}$$

$$\text{At } 500 \text{ probes}/\mu\text{m}^2 \Rightarrow k_{\text{encounter}}^i \approx 1.56 \frac{\text{probes}}{\text{s}} \text{ and } \tau_{\text{encounter}}^i = \frac{1}{k_{\text{encounter}}^i} = 0.64 \text{ s}$$

$$\text{At } 50 \text{ probes}/\mu\text{m}^2 \Rightarrow k_{\text{encounter}}^{ii} \approx 0.156 \frac{\text{probes}}{\text{s}} \text{ and } \tau_{\text{encounter}}^{ii} = \frac{1}{k_{\text{encounter}}^{ii}} = 6.4 \text{ s}$$

$$\text{At } 5 \text{ probes}/\mu\text{m}^2 \Rightarrow k_{\text{encounter}}^{iii} \approx 0.0156 \frac{\text{probes}}{\text{s}} \text{ and } \tau_{\text{encounter}}^{iii} = \frac{1}{k_{\text{encounter}}^{iii}} = 64 \text{ s} \approx 1 \text{ min}$$

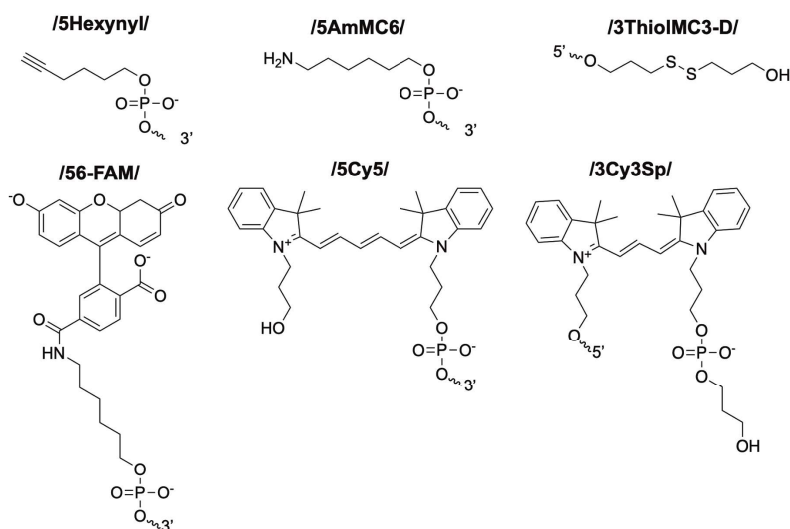
$$\text{At } 0.5 \text{ probes}/\mu\text{m}^2 \Rightarrow k_{\text{encounter}}^{iv} \approx 0.00156 \frac{\text{probes}}{\text{s}} \text{ and } \tau_{\text{encounter}}^{iv} = \frac{1}{k_{\text{encounter}}^{iv}} = 640 \text{ s} \approx 11 \text{ min}$$

Supplementary Note 1. Calculations of the encounter rate for TOI using “turbo-charged” motors. To calculate the encounter rate of the “turbo-charged” motors we used the average speed from triplicate data set (39.10 nm/s). We assumed the density of the RNA fuel on the surface to be 50,000 strands/ μm^2 (ref. 2). Using the depletion track width (~400 nm) and the percent of RNA that is depleted from the depletion track by the turbo-charged motors (~20%), we calculated an encounter rate ($k_{\text{encounter}}$) of 156 strands/s. For example, in surfaces with 500 probes/ μm^2 , the calculated $k_{\text{encounter}}^i$ is 1.56 probes/s and the time ($\tau_{\text{encounter}}^i$) to encounter these probes is 0.64 s.

S3. Supplementary Data

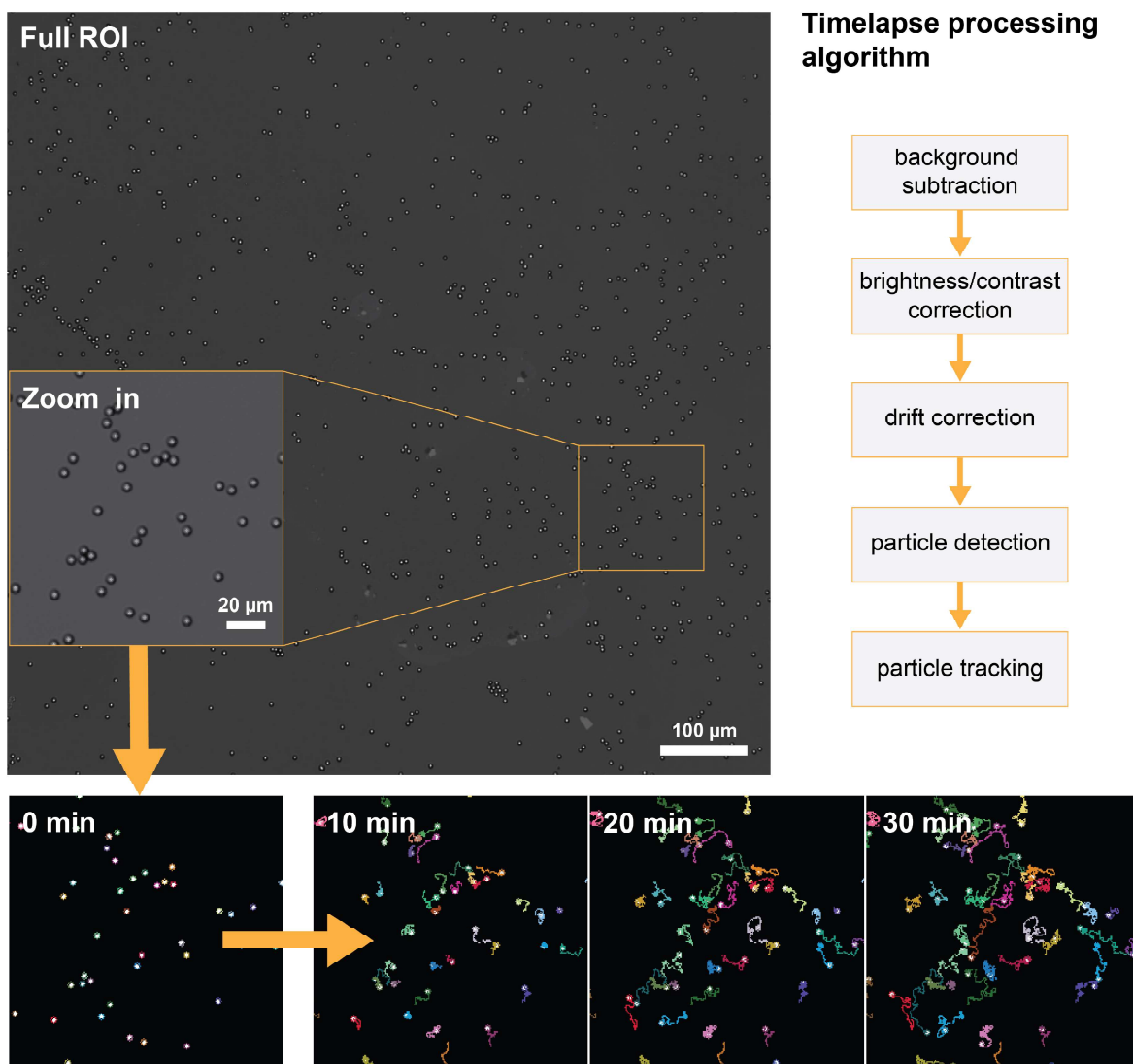
Supplementary Table 1. Oligonucleotide sequences

ID	Sequences (5'-3')
DNA anchor	/5AmMC6/GAGAGAGATGGGTGCTTTTTTTTTTTTTTTT/3ThioMC3-D/
9 bp DNA leg	/5Hexynyl/TTTTTTTTTTTTTTAGTAATCAA
12 bp DNA leg	/5Hexynyl/TTTTTTTTTTTTTTAGTAATCAATCA
15 bp 33% GC DNA leg	/5Hexynyl/TTTTTTTTTTTTTTAGTAATCAATCACAG
18 bp DNA leg	/5Hexynyl/TTTTTTTTTTTTTTAGTAATCAATCACAGGGG
0% GC RNA/DNA chimera	GCACCCATCTCTCTCrCrCrCrCrUrUrArUrArUrArUrArUrArUrU/3Cy3Sp/
0% GC DNA leg	/5Hexynyl/TTTTTTTTTTTTTTAAATATTAATTATAA
0% GC DNA leg v2	/5Hexynyl/TTTTTTTTTTTTTTGGGAAATATTAATTATAA
33% GC RNA/DNA chimera	GCACCCATCTCTCTCrCrCrCrCrUrGrUrGrArUrGrArUrArCrU/3Cy3Sp/
100% GC RNA/DNA chimera	GCACCCATCTCTCTCrCrCrCrCrCrCrGrCrGrGrCrGrGrCrCrCrC/3Cy3Sp/
100% GC DNA leg	/5Hexynyl/TTTTTTTTTTTTTTGGGCGCCGCGCCGCGG
13% GC RNA/DNA chimera	GCACCCATCTCTCTCCCCCCTUrUrArUrGrArUrUrGrArUrArUrU/3Cy3Sp/
13% GC DNA leg	/5Hexynyl/TTTTTTTTTTTTTTAATAATCAATCATAA
15 bp DNA probe	GCACCCATCTCTCTCCCCCCTTATAATTAATATTT/3Cy5Sp/
16 bp DNA probe	GCACCCATCTCTCTCCCCCCTTATAATTAATATTTCC
17 bp DNA probe	GCACCCATCTCTCTCCCCCCTTATAATTAATATTTCC
18 bp DNA probe	GCACCCATCTCTCTCCCCCCTTATAATTAATATTTCCC
17 bp DNA probe with 1 mutation	GCACCCATCTCTCTCCCCCCTTATAATTGATATTTCC
17 bp DNA probe with 2 mutations	GCACCCATCTCTCTCCCCCCTTATAGTTAATGTTTCC
Random DNA strand	GCACCCATCTCTCTCCCCCCTGTGATTGATTACT/3Cy5Sp/
Density reporter	GCACCCATCTCTCTCCCCCCTGTGATTGATTACT
Thiolated DNA	/5ThioMC6-D/TTTAGTAATCAATCACGG/3AmMO/



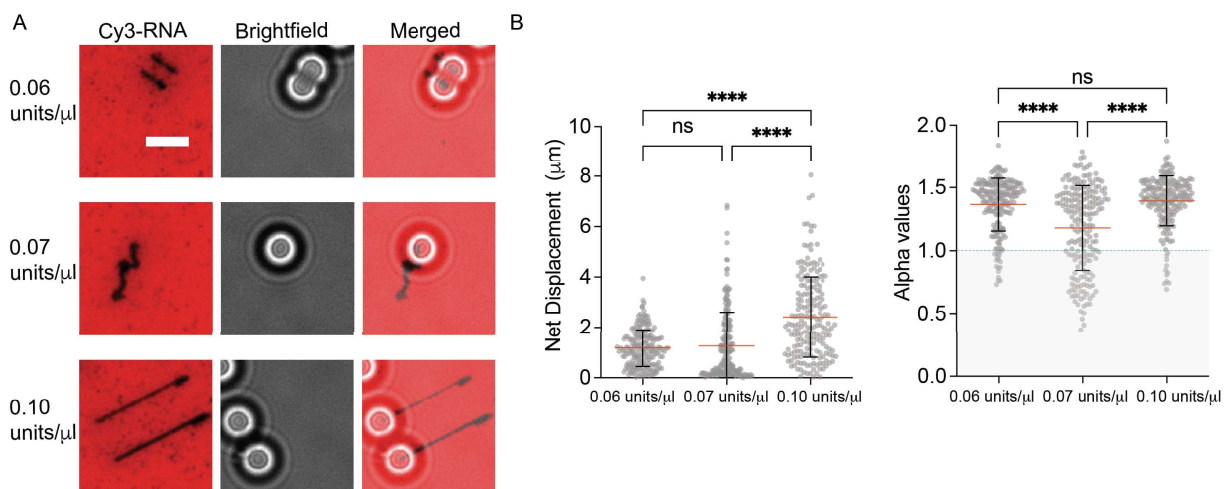
Supplementary Table 1. Table summarizing the sequences of oligonucleotides used in the design of rolling DNA motors. The sequences are displayed in a 5' to 3' orientation. The 3' and 5' DNA and RNA modifications are indicated in the table and illustrated below it.

Supplementary Figure 1



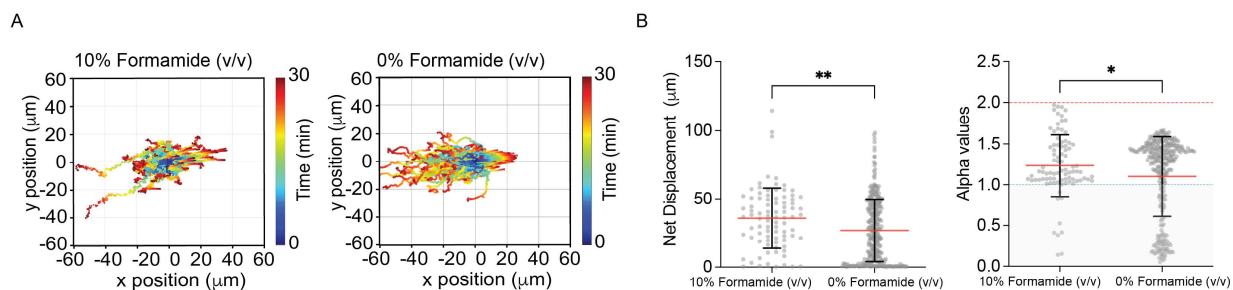
Supplementary Figure 1. Image processing and localization of DNA-based motors via the MOSAIC particle tracker suite^[3]. The MOSAIC algorithm was used for particle detection. The flowchart shows processing steps for acquiring localizations and tracking of 5 μm DNA-based motors based on brightfield imaging. Image processing steps include background subtraction along with brightness/contrast correction. Drift correction is then performed followed by particle detection and tracking (MOSAIC suite). Brightfield overlay of particles with color-coded trajectories at $t = 0, 10, 20,$ and 30 min.

Supplementary Figure 2



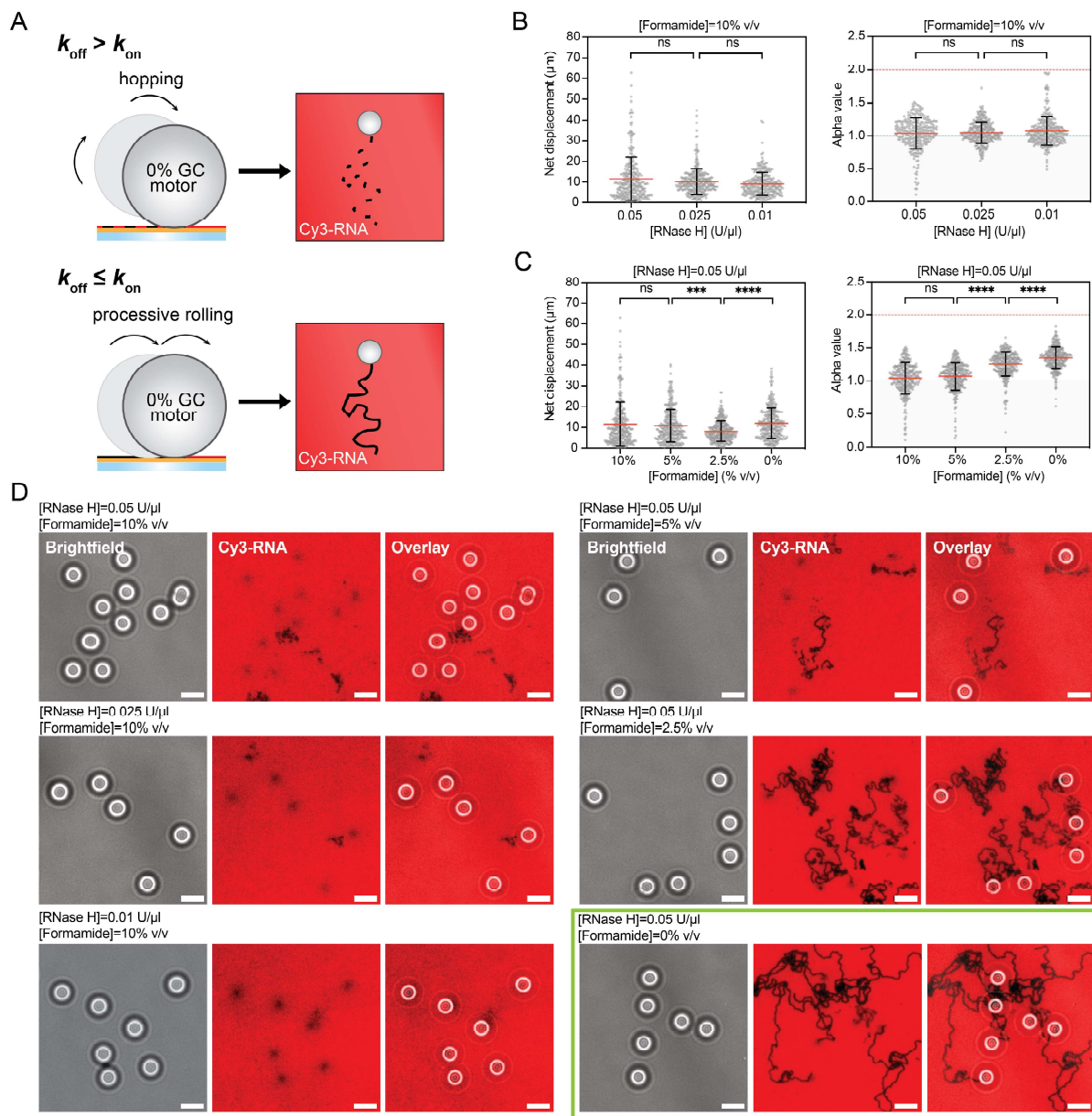
Supplementary Figure 2. Analyzing the performance of 18 bp DNA-based motors. **A)** Representative fluorescence and brightfield imaging along with merged images of the DNA-based motors modified with leg lengths of 18 bp and their depletion tracks. The motors were incubated with different RNase H concentrations: 0.06, 0.07, 0.10 units/ μ l and imaged 30 mins after RNase H addition. The RNA fuel was tagged with Cy3, shown here in red. The scale bar is 5 μ m. **B)** Plots showing **(left)** net displacements and **(right)** α values of 300 motors modified with 18 bp DNA legs at different RNase H concentrations (0.06, 0.07, 0.10 units/ μ l). ns and **** indicate not statistically significant and $P < 0.0001$, respectively.

Supplementary Figure 3



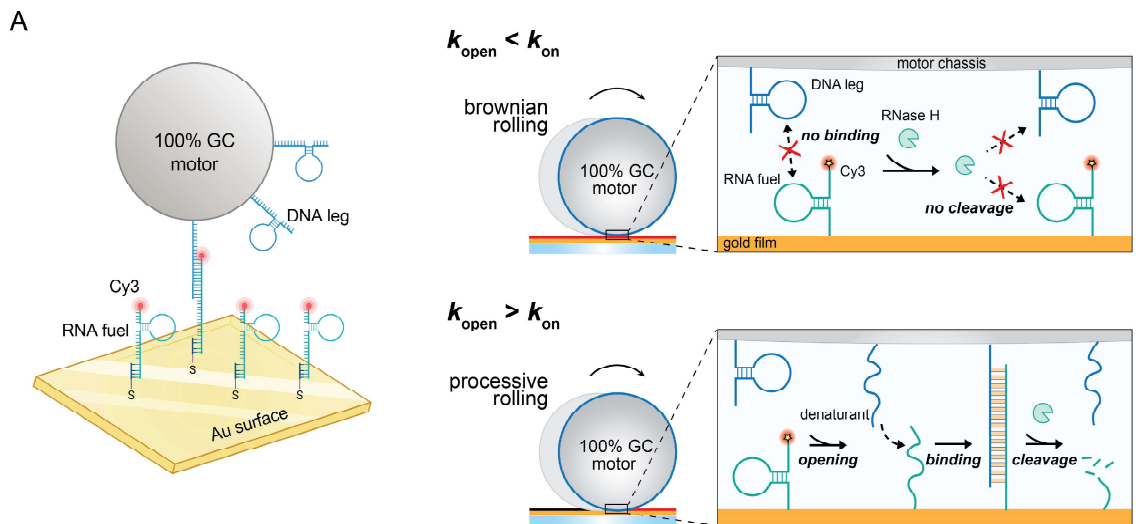
Supplementary Figure 3. Analyzing the performance of 9 bp DNA-based motors. **A)** Plots showing the trajectories of 100 motors modified with 9 bp DNA legs incubated in buffer containing 10% and 0% formamide (v/v). All the trajectories are aligned to the 0,0 (center) of the plots for time = 0 min. Color indicates time (0 \rightarrow 30 min). **B)** Plots showing **(left)** net displacements and **(right)** α values of ≥ 100 motors modified with 9 bp DNA legs. * and ** indicate $P < 0.05$ and $P = 0.0014$, respectively.

Supplementary Figure 4



Supplementary Figure 4. Optimization of 0% GC motors. **A**) Schematic of 0% GC motor motion. If $k_{\text{off}} > k_{\text{on}}$, the 0% GC exhibits a hopping behavior and does not form continuous Cy3-RNA depletion tracks. This is in contrast to $k_{\text{off}} < k_{\text{on}}$ in which the 0% GC motor rolls processively on the RNA monolayer forming continuous depletion tracks. **B**) Plots showing (left) net displacements and (right) α values of 300 motors with 0% GC base pairs at different RNase H concentrations and 10% formamide (v/v). ns indicates not statistically significant. **C**) Plots showing (left) net displacements and (right) α values of 300 motors with 0% GC base pairs incubated with 5 units/ μl of RNase H and different concentrations of formamide. ns, ***, and **** indicate not statistically significant, $P=0.001$, and $P<0.0001$, respectively. **D**) Representative fluorescence and brightfield imaging along with merged images of the 0% GC motors and their depletion tracks. The motors were incubated with the enzyme and formamide concentrations reported in (B) and (C). The optimal buffer conditions of 0.05 units/ μl and 0% formamide (v/v) are outlined in green as the motors under these conditions are highly processive and form long, continuous depletion tracks in the Cy3-RNA channel. The scale bar is 5 μm .

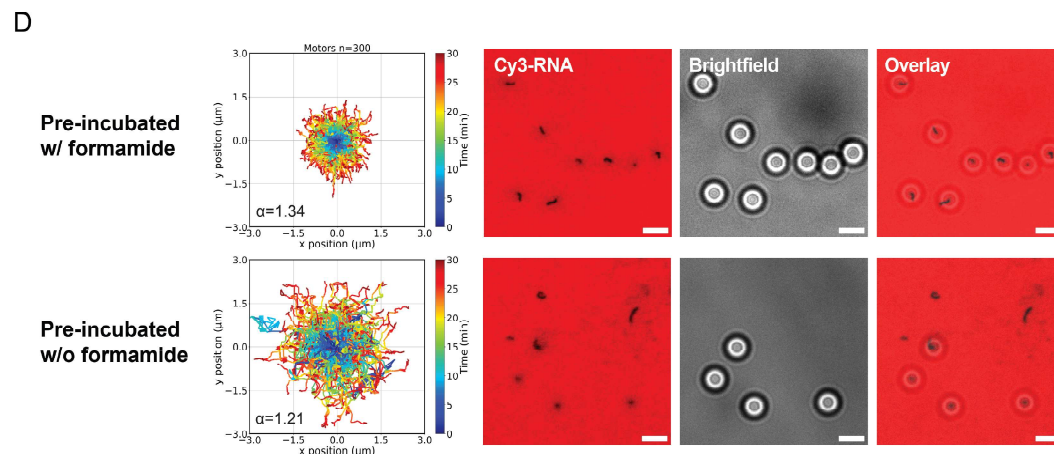
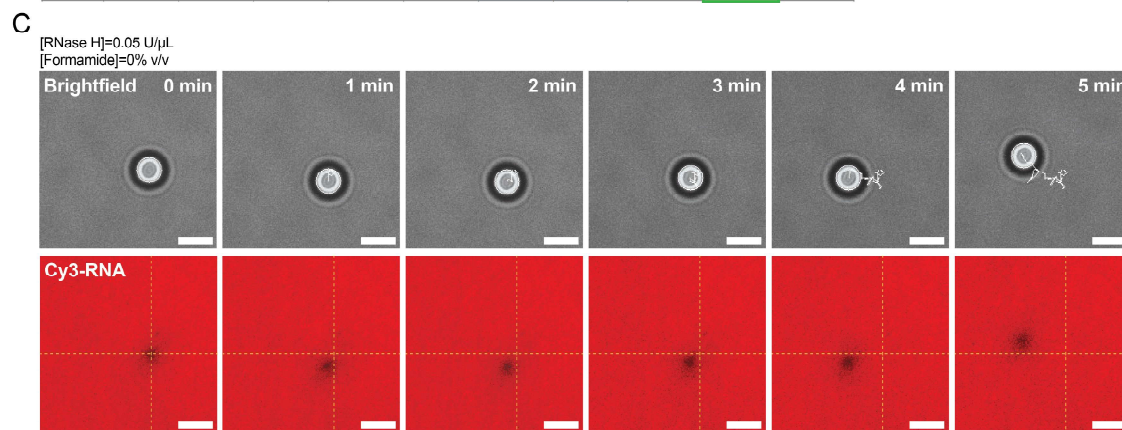
Supplementary Figure 5



B

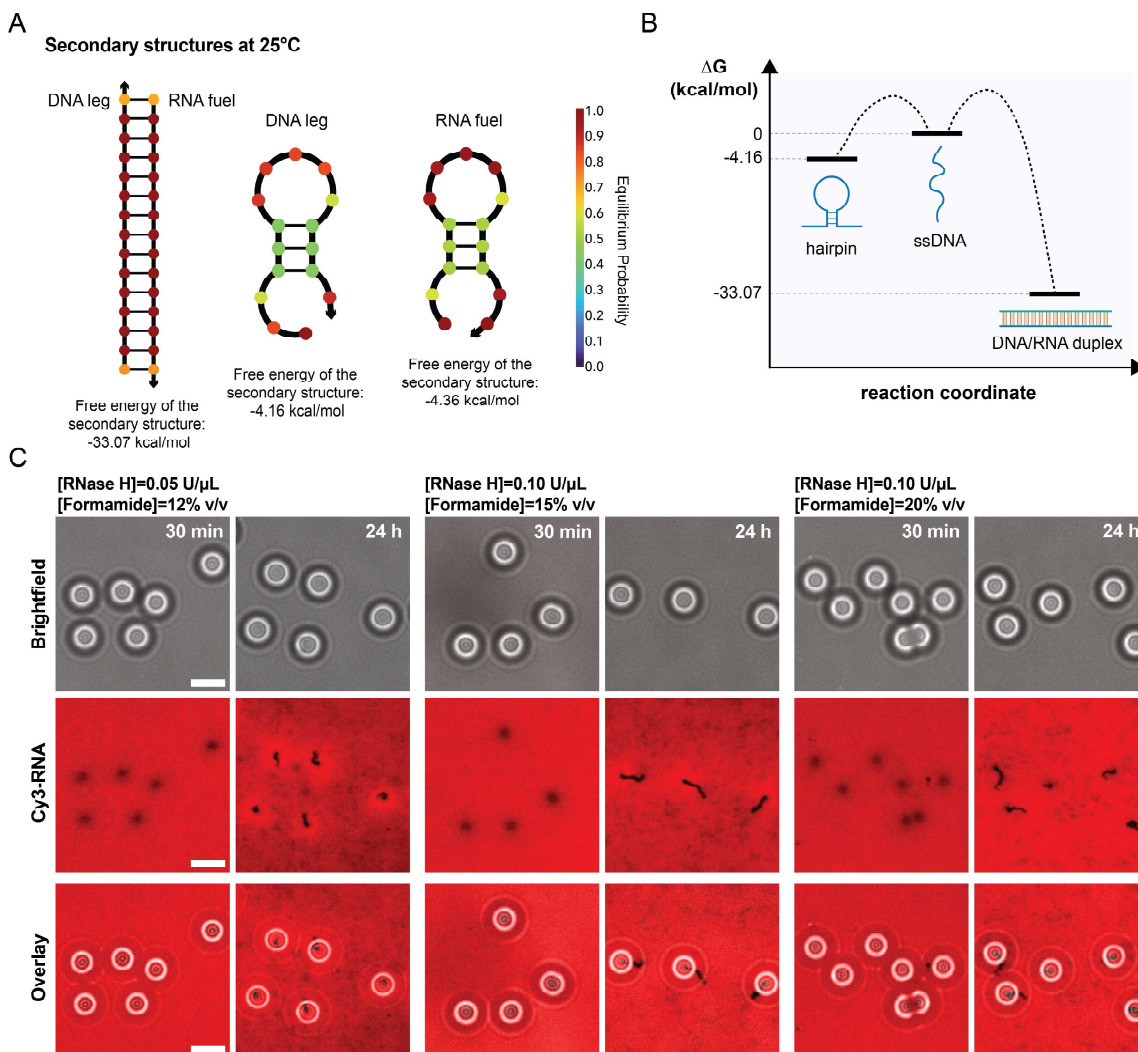
avg. net displ. avg. α value		[Formamide] (% v/v)								
		0	2.5	10	12	15	20	25	30	35
[RNase H] (units/ μ L)	0.025	-	-	-	-	0.303 μ m $\alpha=0.793$	-	0.192 μ m $\alpha=0.727$	0.612 μ m $\alpha=1.23$	0.519 μ m $\alpha=1.102$
	0.05	9.442 μ m $\alpha=1.046$	3.145 μ m $\alpha=0.826$	1.218 μ m $\alpha=0.875$	0.757 μ m $\alpha=0.840$	-	-	1.621 μ m $\alpha=0.829$	0.640 μ m $\alpha=1.269$	-
	0.10	-	-	-	-	1.52 μ m $u=0.883$	2.687 μ m $u=0.859$	-	0.967 μ m $u=1.329$	-

w/o pre-incubation with formamide
w/ pre-incubation with formamide
- Not tested



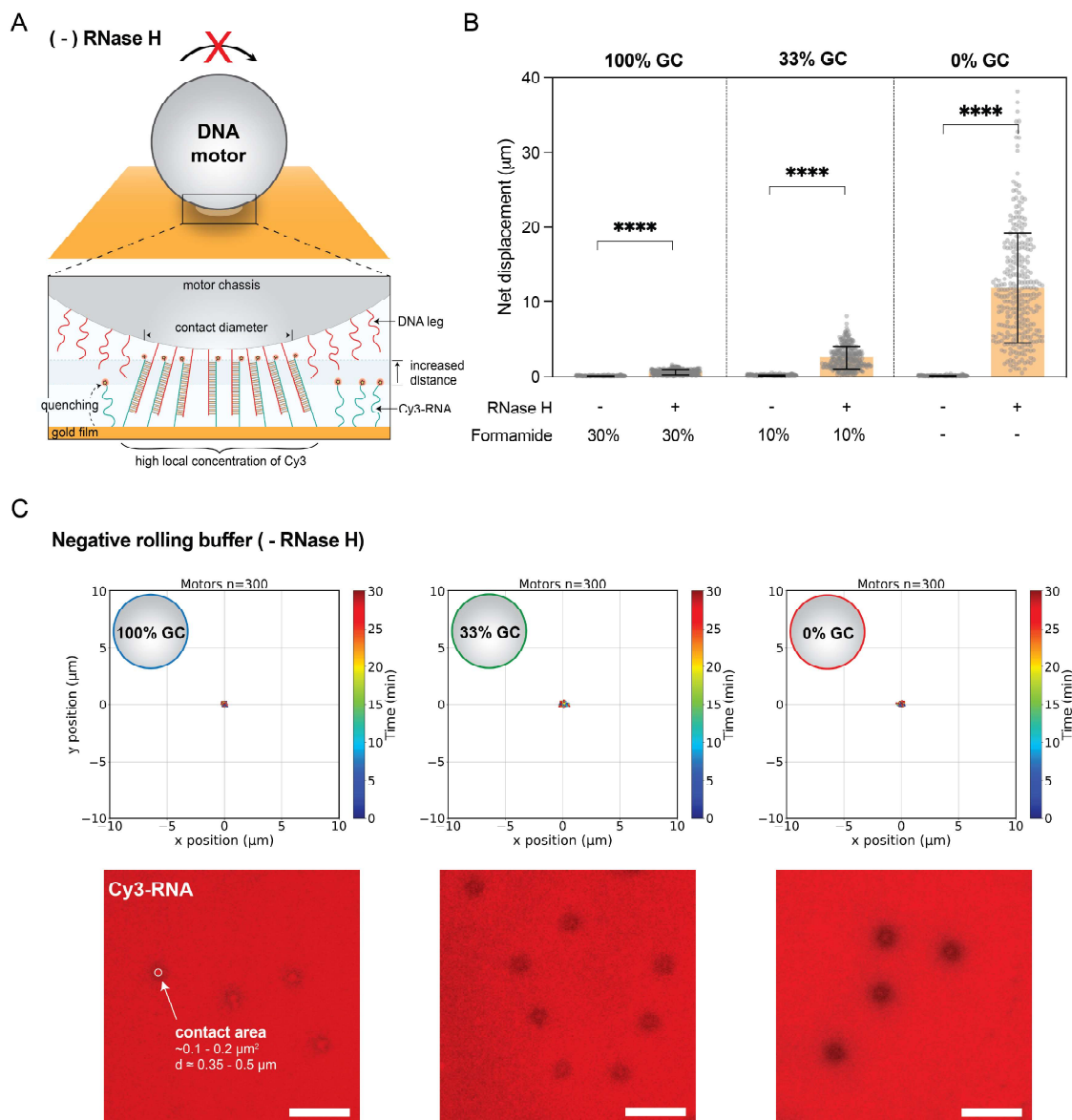
Supplementary Figure 5. Optimization of 100% GC motors. A) Scheme of 100% GC motor motion. The 100% GC motors form secondary structures which prevent the DNA legs from binding to the RNA fuel thus hindering processive motion and leading to Brownian motion instead. For processive rolling to occur, the secondary hairpin structures must open (with the help of a denaturant) allowing for binding between the DNA leg and RNA fuel. **B)** Table summarizing the screening of different buffer conditions and the motor performance in terms of average net displacement and α value. The screening also includes conditions in which the motors were pre-incubated with 20% formamide (v/v) in 1x PBS before initiating motion. The optimal buffer conditions for 100% GC motor motion are outlined in green in which the motors are pre-incubated with 20% formamide (v/v) in addition to 30% formamide (v/v) in the rolling buffer. **C)** Representative fluorescence and brightfield imaging of the 100% GC motors over the course of 5 mins. The motors were incubated with 0.05 units/ μ l RNase H and 0% formamide (v/v). The scale bar is 5 μ m. **D)** Plots showing the trajectories of 100% GC motors pre-incubated with and without 20% formamide (v/v) in 1x PBS. All the trajectories are aligned to the 0,0 (center) of the plots for time = 0 min. Color indicates time (0 \rightarrow 30 min). The average α value for motors pre-incubated with formamide is 1.34 and that of motors without formamide preincubation is 1.21. Scale bar is 5 μ m.

Supplementary Figure 6



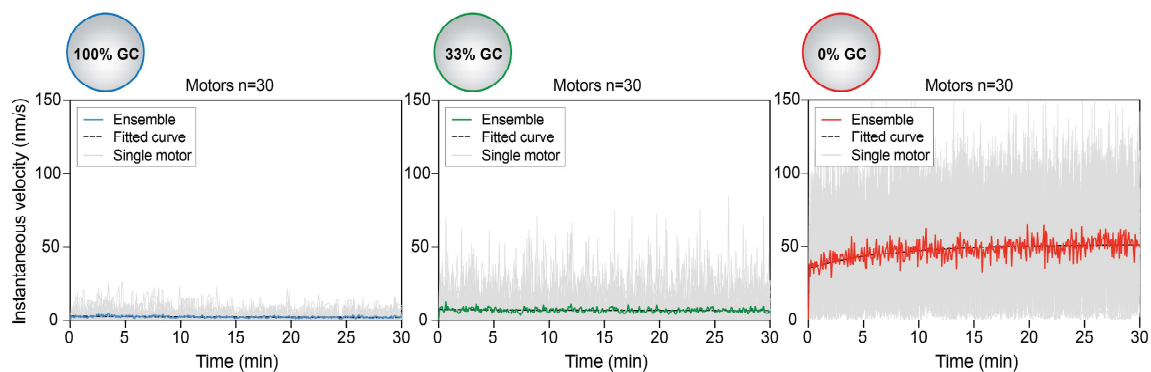
Supplementary Figure 6. Thermodynamic properties of 100% GC motors. **A)** Secondary structures of a 1:1 mixture of 100% GC DNA leg and the complementary RNA foothold at 25°C predicted using NUPACK (<http://www.nupack.org/>). The arrows represent the 3' end of the oligonucleotides, and the nucleotides are color-coded by their equilibrium probability (legend on right). **B)** Reaction coordinate diagram showing the relative stability of the thermodynamic product formed by the hybridization of DNA legs with RNA footholds and the kinetic product that result from the intramolecular folding of ssDNA. **C)** Representative brightfield and fluorescence imaging along with merged images of the 100% GC motors collected after 30 min and 24 h incubation in rolling buffers prepared with formamide concentrations below the optimized threshold of 30% (v/v) for processive rolling. Track formation does not occur in the first 30 min of rolling because of kinetic traps that can unfold over time and be supplanted by the thermodynamic product, allowing the detection of depletion tracks after 24 h. The scale bar is 5 μm.

Supplementary Figure 7



Supplementary Figure 7. Motor translocation is initiated by RNase H enzyme addition. A) Illustration of motor binding to the RNA monolayer and remaining stationary as no chemical gradient is generated in the absence of RNase H. **B)** Plot of net displacement distributions of DNA motors with varying GC content in the absence and presence of RNase H at the optimized formamide concentration for each motor design. **C)** Ensemble of 300 motor trajectories plotted from the center (0, 0) with representative fluorescence images in the Cy3-RNA channel showing no depletion tracks regardless of the GC content. The fluorescence intensity below the motor chassis is reduced as a result of a change in the refractive index and the contact area can be measured by the bright center generated by the high local concentration of Cy3 that is stretched farther from the quenching gold film. Scale bar is 5 μm .

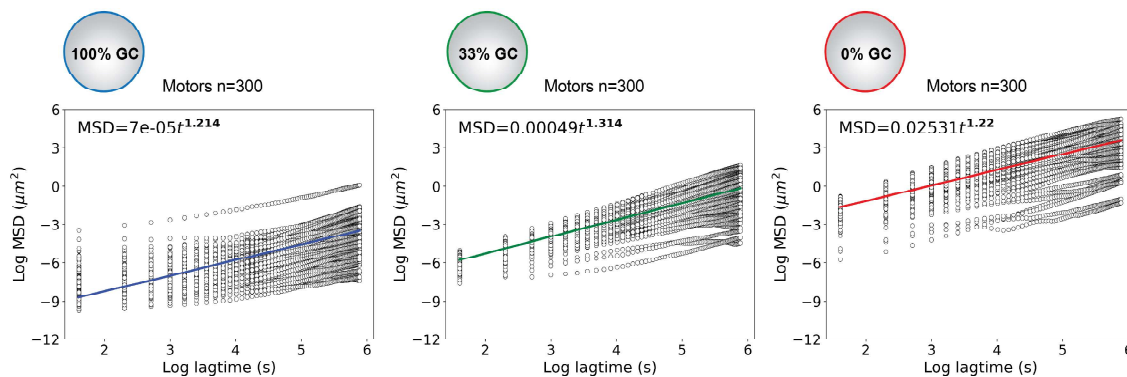
Supplementary Figure 8



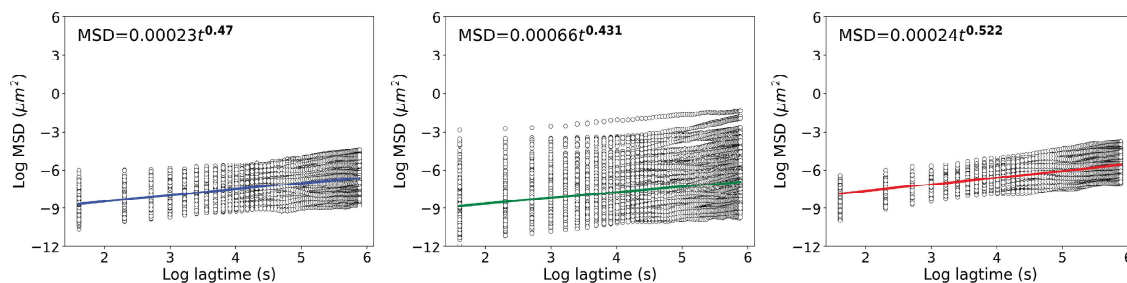
Supplementary Figure 8. Motors with varying GC content travel at different speeds. Plots showing the instantaneous velocity over time for 30 individual motors (gray lines) and the respective ensemble at 100% (blue), 33% (green) and 0% (red) GC content in the leg-foothold duplex. The instantaneous velocity is given by the traveled distance divided by the time interval between consecutive frames (5 sec). The frame rate is 0.2 Hz.

Supplementary Figure 9

(+) RNase H

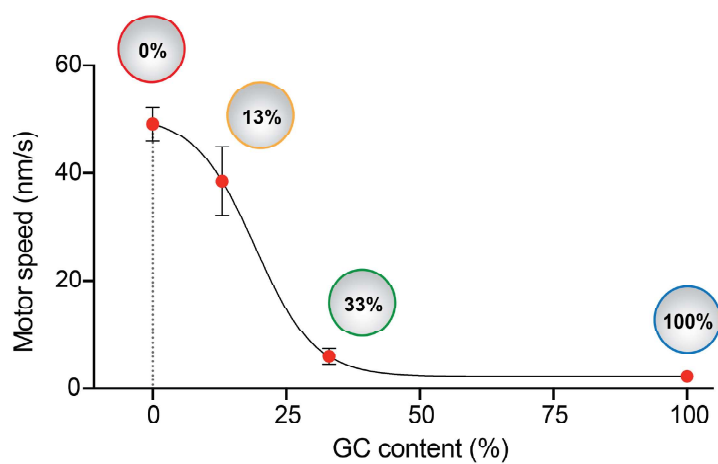


(-) RNase H



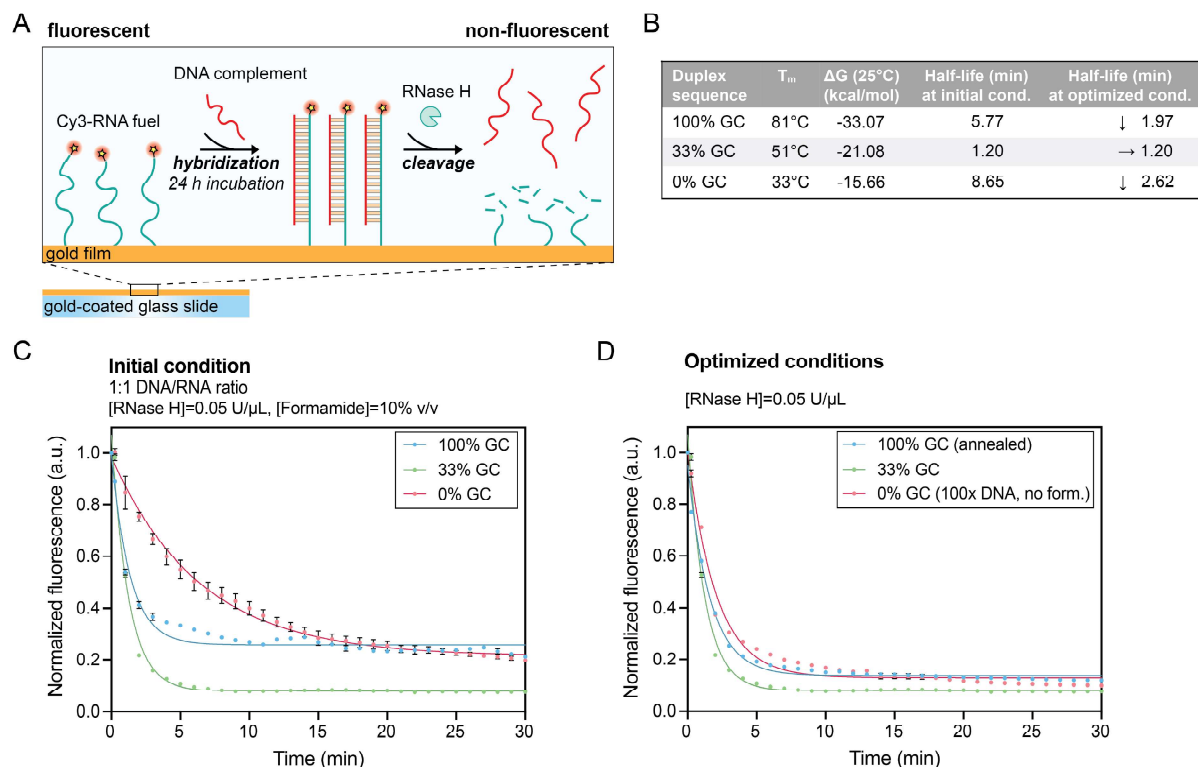
Supplementary Figure 9. Motors with varying GC content can all travel in a superdiffusive manner when propelled by RNase H. Plot of MSD as a function of lagtime on a logarithmic scale for 300 individual motors of varying GC content, providing the alpha value from the power law dependence. Motion is superdiffusive ($\alpha > 1$) only in the presence of the propelling agent RNase H while subdiffusive alpha values ($\alpha < 1$) are recorded for stationary motors in the absence of RNase H.

Supplementary Figure 10



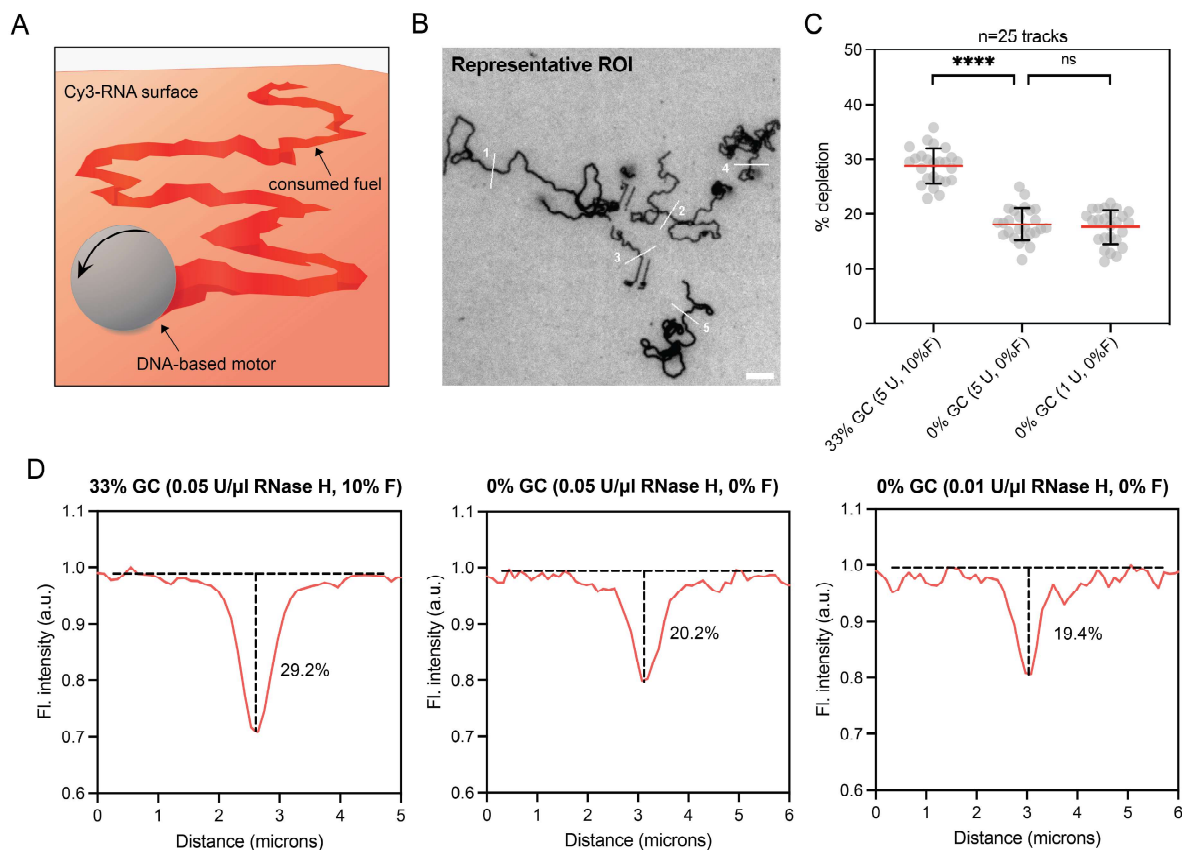
Supplementary Figure 10. Dependence of motor speed on the GC content of the DNA leg-RNA foothold duplex. Plot of average motor speed as a function of GC content with non-linear fitting of experimental values using a sigmoidal function ($R^2=1.0$). The error bars represent the standard deviation from 300 individual motors.

Supplementary Figure 11



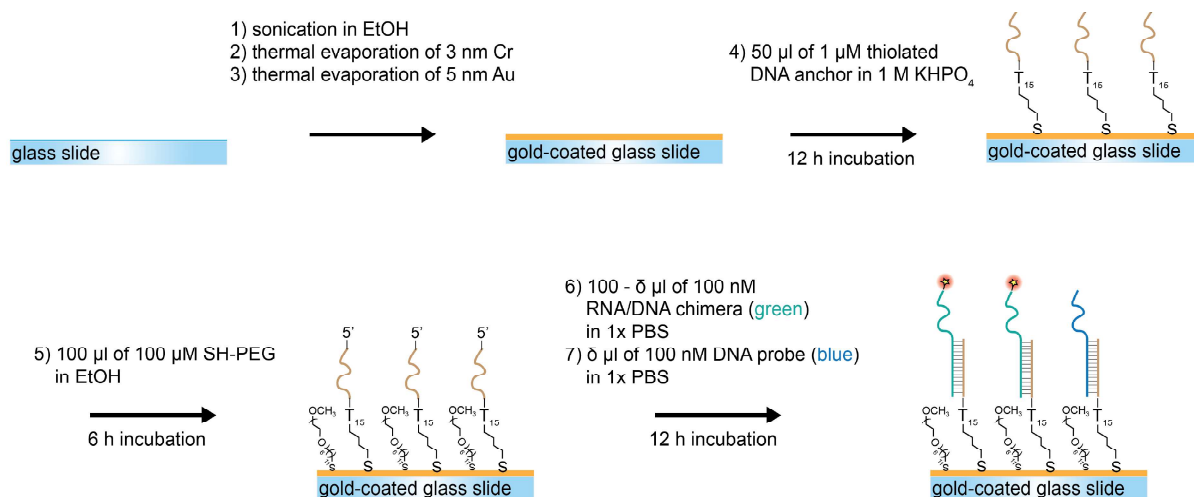
Supplementary Figure 11. Kinetic measurements of RNase H activity at varying GC content in the duplexed RNA substrate. **A)** Schematic of surface immobilization of Cy3-labeled RNA fuel hybridized overnight with the complementary DNA strand and hydrolyzed by RNase H to determine the rate of enzymatic activity. **B)** A table summarizing the results of the kinetic measurements of enzymatic activity on duplexed RNA substrate of varying GC content. Half-life of the reaction was calculated by fitting the fluorescence decay plots in (C) and (D) to an exponential decay function. **C)** Kinetic plots showing RNase hydrolysis at the same initial condition and **D)** at optimized condition for each type of surface. The formation of hairpin structures at 100% GC and the spontaneous dissociation at 0% GC are responsible for lowering the substrate concentration, leading to slower enzymatic activity compared to the one observed at 33% GC. Similar half-life times are instead recorded upon annealing and introducing 100 times excess of DNA complement as well as withholding formamide for the 100% GC and 0% GC designs, respectively. The error bars represent the standard deviation in the average fluorescence intensity from 5 different regions across the reaction chamber.

Supplementary Figure 12



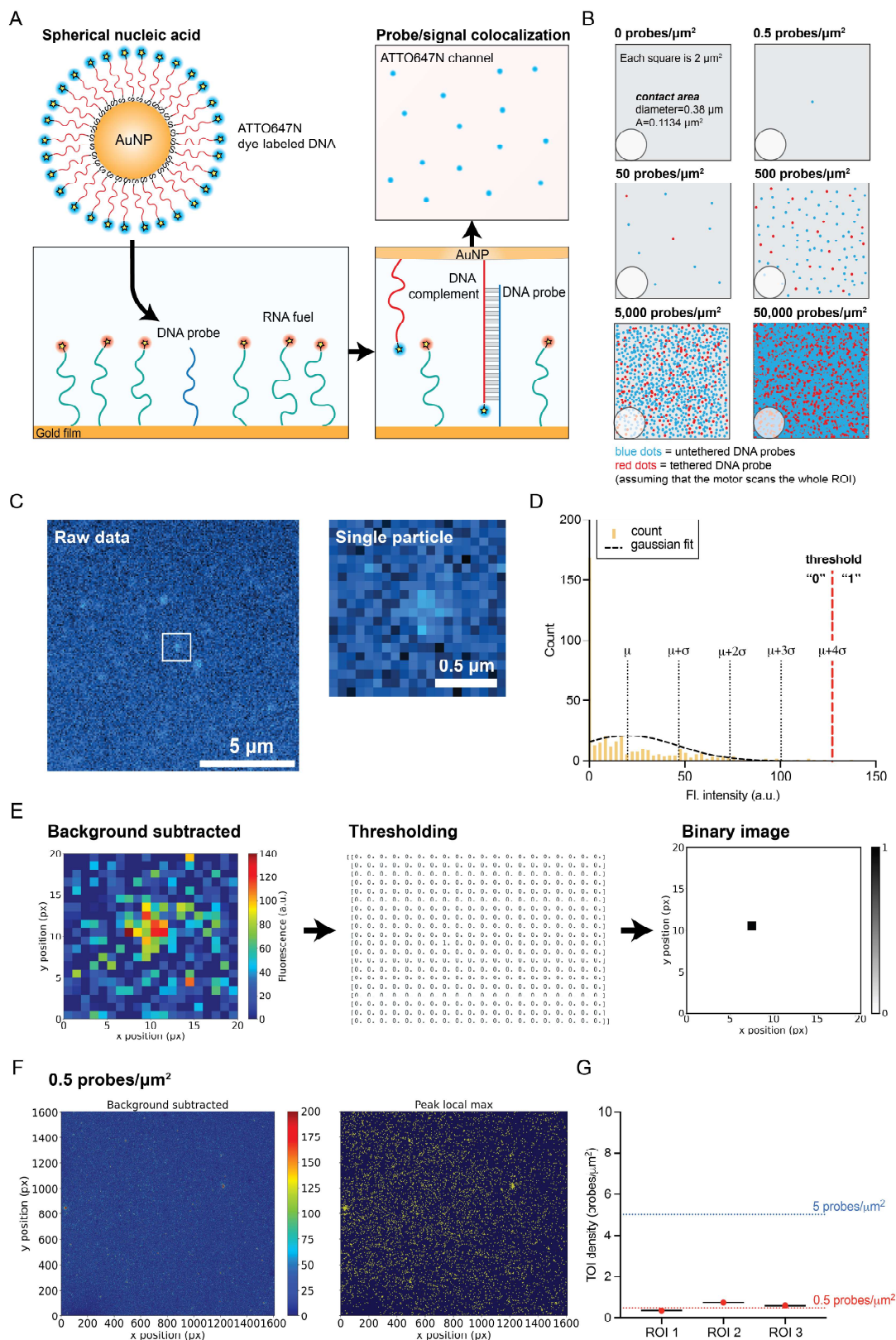
Supplementary Figure 12. Quantification of fuel consumption through the analysis of depletion tracks. A) Illustration of a DNA-based motor generating a depletion track by consuming chemical fuel in the form of RNA along its path. **B)** Representative Cy3-RNA fluorescence image showing depletion tracks that confirm the burnt-bridge mechanism of motor translocation. Scale bar is 5 μ m. **C)** Plot of percentage of fuel depletion within the wake of ($n=25$) individual depletion tracks for 33% GC motors (0.05 U/ μ l RNase H and 10% v/v formamide) and 0% GC motors at 0.05 and 0.01 U/ μ l RNase H (0% v/v formamide). **D)** Representative line scans from each of the conditions listed in (C). Turbo-charged motors at 0% GC consume approx. 20% of the RNA fuel in the contact area, suggesting a lower number of DNA-RNA junctions compared to the 33% GC motors.

Supplementary Figure 13



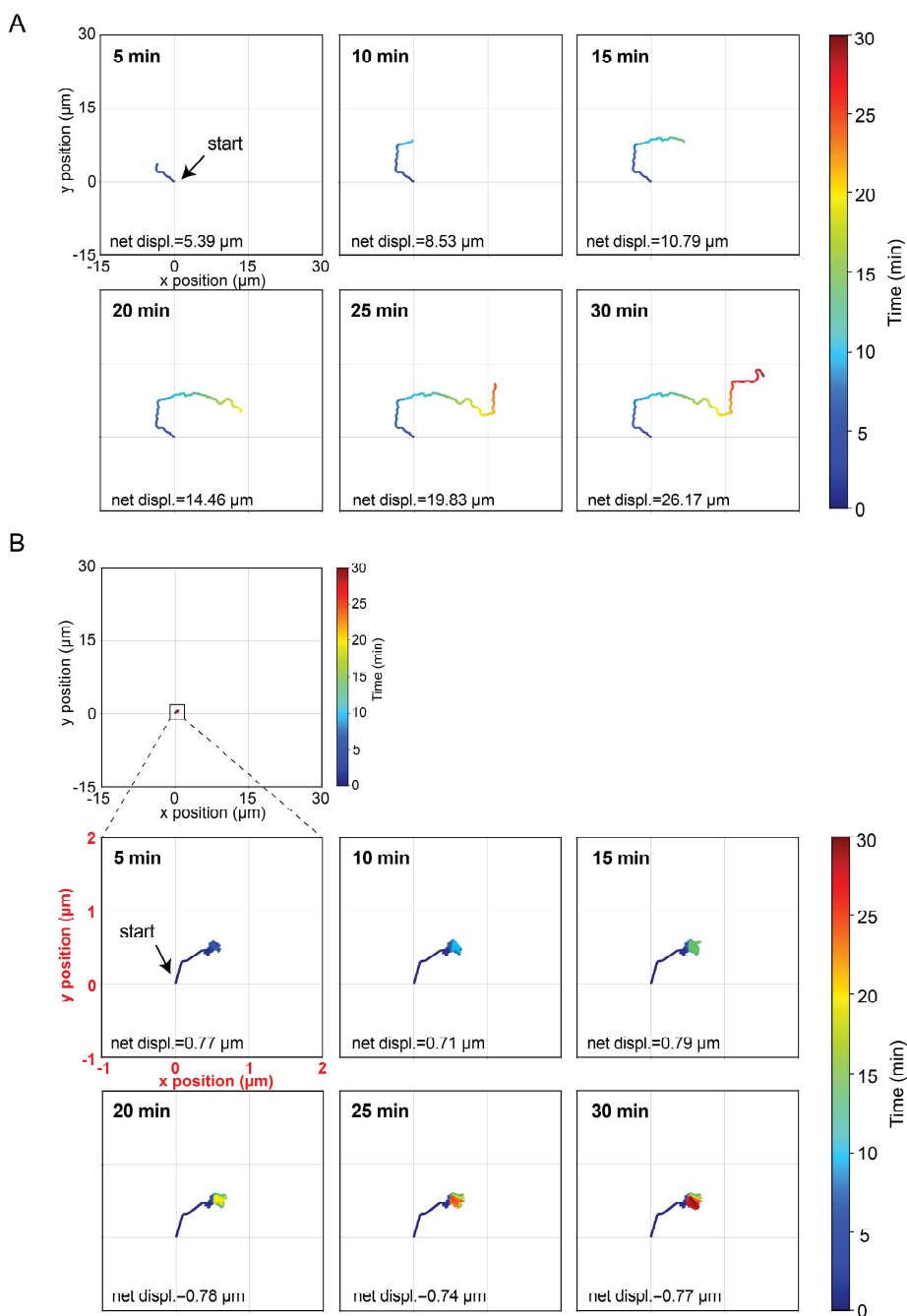
Supplementary Figure 13. Fabrication of RNA-DNA probe monolayer. Schematic of the surface preparation steps used for preparing RNA-DNA probe monolayer surface. Following the deposition of 3 nm of chromium (Cr) and 5 nm of gold (Au) via thermal evaporation, the surface was treated with 1 μ M of thiolated DNA anchor strand in 1 M KPi. After 12 hours of incubation, the surface was passivated using 100 μ M thiolated polyethylene glycol (PEG) for 6 hours to prevent non-specific binding of RNase H to the surface. Then Cy3-labeled RNA/DNA chimera and different ratios of DNA probe were added to hybridize with the DNA anchor on the gold film to obtain surfaces of varying densities of target DNA.

Supplementary Figure 14



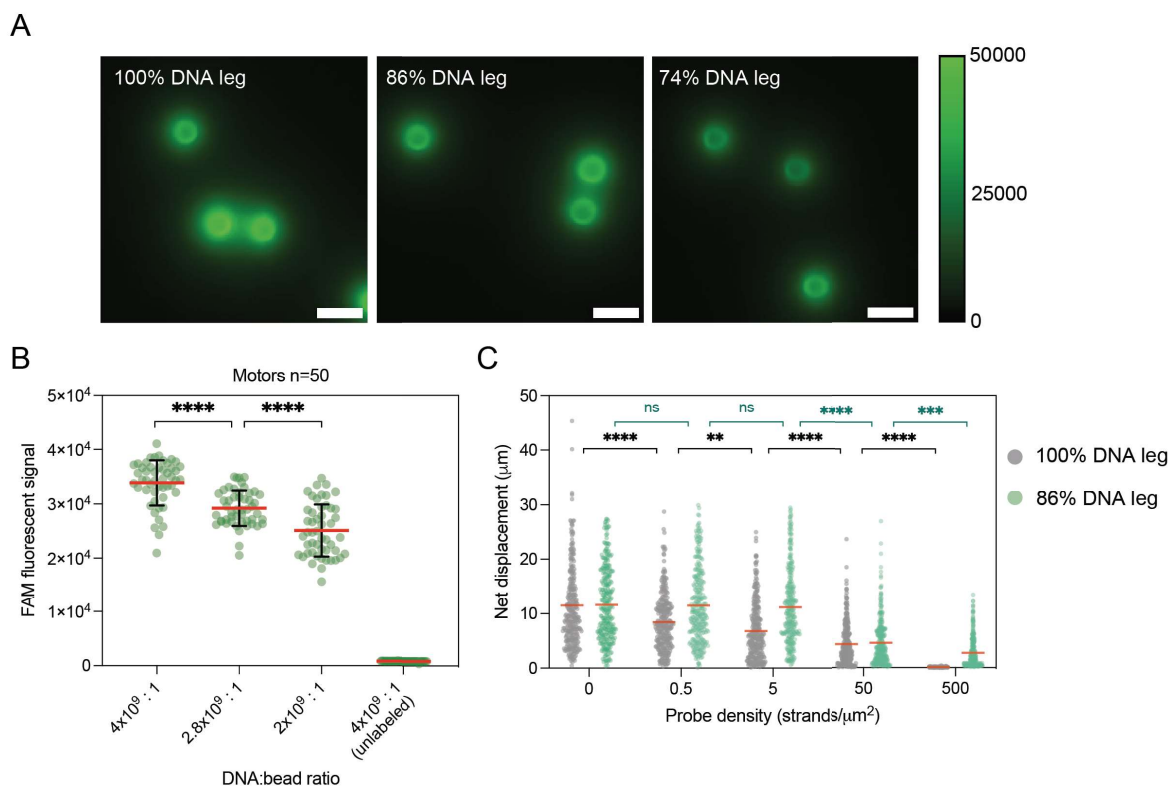
Supplementary Figure 14. Fluorescence signal generation for visualizing the surface probe distribution. A) Schematic of fluorescent signal generation coinciding with the target DNA strands using spherical nucleic acids functionalized with complementary ATTO647N-labeled DNA. **B)** Hypothetical probe distribution in a $2\text{-}\mu\text{m}^2$ region that contain the contact area between a $5\text{-}\mu\text{m}$ motor particle and the surface, drawn to scale. Each dot represents a DNA probe, and the color indicates whether it is untethered (blue) or tethered (red) to a motor assuming that the whole ROI is scanned and $\sim 20\%$ of surface strands, including the RNA footholds, are tethered. **C)** Visual identification of a single SNA particle from a raw fluorescence image of a $0.5\text{ probes}/\mu\text{m}^2$ surface. **D)** Representative histogram of the fluorescence intensity values (subtracted from background fluorescence intensity in the image) of the selected zoom-in region in (C). A normal distribution was fitted to the fluorescence intensity values, and the threshold for the peak local maximum was determined as four standard deviations above the mean. **E)** Image processing algorithm for converting the fluorescence image into a binary image using the threshold determined in (D). Each pixel is color-coded by fluorescence intensity. **F)** Detection of peak local maxima associated with SNA binding in a full region of interest of the $0.5\text{ probes}/\mu\text{m}^2$ surface using the algorithm shown in (E). **G)** Plot showing the calculated target probe density in three separate regions of interest that closely match the predicted density ($0.5\text{ probes}/\mu\text{m}^2$).

Supplementary Figure 16



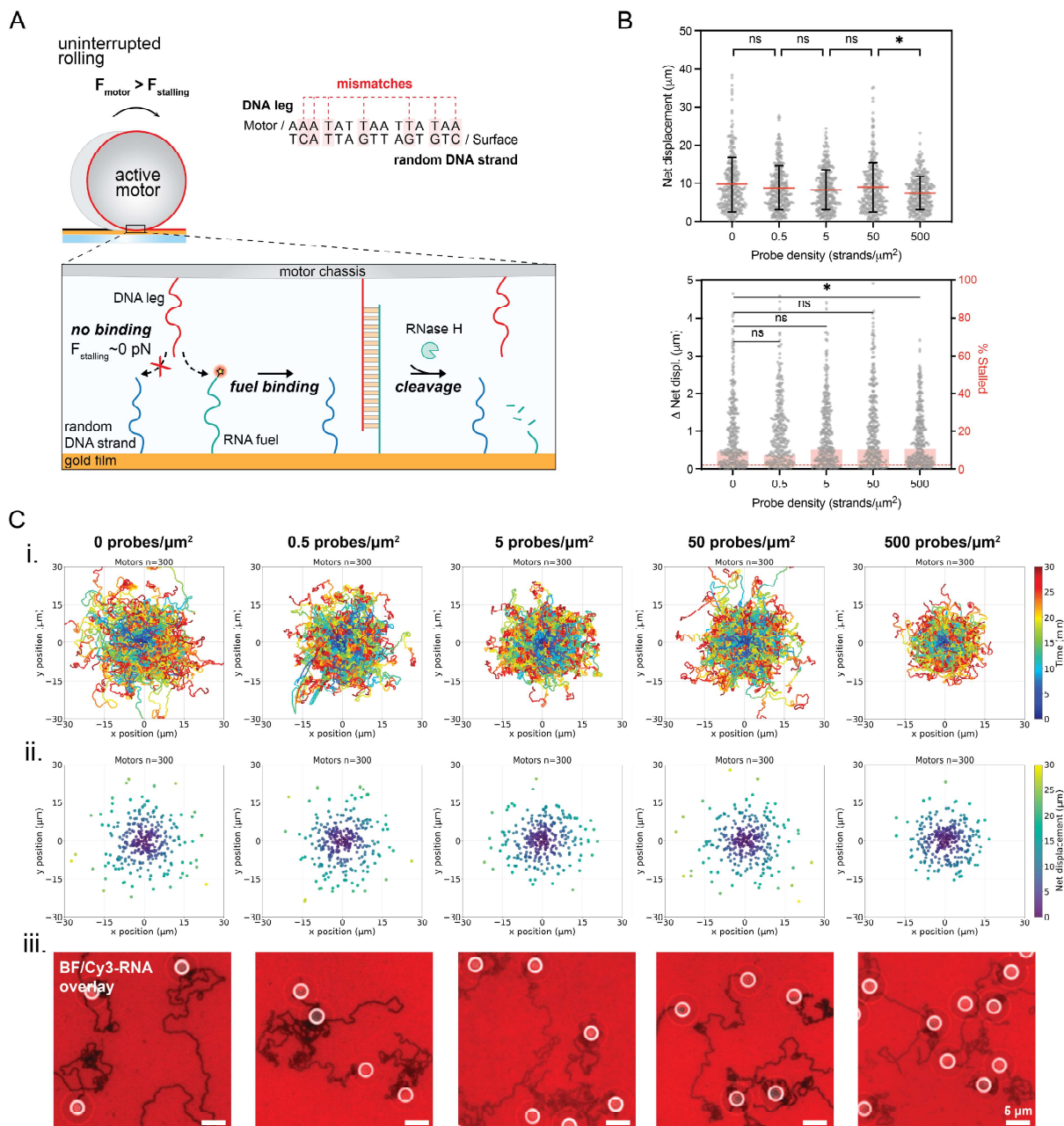
Supplementary Figure 16. Determination of stalling time and position from single-particle trajectories. Representative motor trajectory plotted from the (0, 0) position at time = 0 min on a surface containing **(A)** 0 probes/ μm^2 which represents the control and **(B)** 500 probes/ μm^2 . Color indicates time (0 \rightarrow 30 min). If the motor never encounters a target DNA probe, its trajectory grows without interruption, and the corresponding net displacement increases over time. Meanwhile, the encounter and binding to one or more DNA probes lead to motor stalling, as indicated by the unvaried motor coordinates and the color at the tip of the trajectory changing at different time points.

Supplementary Figure 18



Supplementary Figure 18. Effect of DNA leg density on LOD. A) Representative fluorescence images of motors functionalized with FAM-labelled DNA legs at different leg density. Scale bar is 5 μm . **B)** Plot of FAM fluorescent signal generated by mixing different ratios of FAM-labeled DNA legs and motor beads to quantify the variation in the DNA leg density. **C)** Comparative plots showing net displacement of 300 motors with varying DNA leg density on surfaces containing 0, 0.5, 5, 50, and 500 probes/ μm^2 . ns, ** and **** indicate not statistically significant, $P=0.0031$ and $P<0.0001$, respectively. The error bars and the red lines represent the standard deviation and the mean of the distribution, respectively.

Supplementary Figure 19



Supplementary Figure 19. Specificity of the mechanical readout. A) Schematic of motion response to non-complementary DNA probes. Since the DNA legs cannot bind to the random DNA strand, no stalling force is generated, and motion occurs without opposing resistance. **B) (top)** Plot showing net displacement of 300 motors on surfaces containing 0, 0.5, 5, 50, and 500 probes/ μm^2 . ns and * indicate not statistically significant and $P < 0.05$, respectively. The error bars and the red lines represent the standard deviation and the mean of the distribution, respectively. **(bottom)** Plots of the Δ net displacement as well as the percentage of motors stalled in the final 2 minutes of the 30-minute time lapse ($t = 28$ – 30 min) for 300 motors on surfaces containing 0, 0.5, 5, 50, and 500 probes/ μm^2 . The red-dashed line represents the threshold ($0.100 \mu\text{m}$) used to calculate the percentage of stalled motors. * indicates $P < 0.05$. **C)** (i) Plots showing the trajectories of 300 motors challenged by increasing densities of DNA probe. All the trajectories are aligned to the 0,0 (center) of the plots for time = 0 min and color indicates time (0 \rightarrow 30 min). (ii) Plots showing the final position of each trajectory in (i) after 30 min rolling. Each dot is color-

coded by net displacement. **(iii)** Representative overlay of brightfield and fluorescence imaging of motors colocalized with long depletion tracks (at $t = 30$ min after RNase H addition).

S4. Supplementary Movies

Supplementary Movie 1. Timelapse video of the trajectories created by 0%, 33%, and 100% GC motors. The trajectories are centered at (0,0) and color-coded to indicate time. The trajectories were created using the x and y positions of the motors from brightfield particle tracking.

Supplementary Movie 2. Timelapse videos of Cy3 (red) fluorescence channels overlaid with brightfield acquired at 5 s intervals for a duration of 5 mins. The video was acquired ~30 mins after RNase H addition using a 100x 1.49 NA objective. On the **left** is the 33% GC motor and on the **right** is the 0% GC motor. The depletion tracks created by each motor are shown in black. Scale bar is 5 μm .

References

- [1] B. Liu, J. Liu, *J. Am. Chem. Soc.* **2017**, *139*, 9471–9474.
- [2] K. Yehl, A. Mugler, S. Vivek, Y. Liu, Y. Zhang, M. Fan, E. R. Weeks, K. Salaita, *Nat. Nanotechnol.* **2016**, *11*, 184–190.
- [3] I. F. Sbalzarini, P. Koumoutsakos, *J. Struct. Biol.* **2005**, *151*, 182–195.